University of Padova

DEPARTMENT OF PHYSICS AND ASTRONOMY "GALILEO GALILEI"

Undergraduate degree in Astronomy

Bachelor Thesis in Astronomy

Correlation between neutrinos and jetted AGN

Candidate:
Leonardo Gastaldello

Supervisor:
Mauro D'Onofrio

Co-Supervisor:
Paola Marziani

Academic Year 2022-2023

Physics is like music. The question isn't how to write it, but whether you feel it. Can you?

Semicit.

Abstract

After a brief introduction to the structure of the jetted (or radio-loud) Active Galactic Nuclei (AGN), we talk about the evidence of relativistic components in the jets. Then we talk about their empirical classification and the hint that brings scientists to a generic unified classification, in particular for the jetted ones. We present the two main models to explain their Spectral Energy Distribution (SED), that is the leptonic and the lepto-hadronic model, in which the principal responsible of the high energy part of the SED are respectively electrons or protons. In these models, the acceleration of the particles takes place in the inner part of the AGN jet, acceleration that is caused by the electromagnetic field formed by the Super Massive Black Hole (SMBH), located in the center of the AGN. When protons become relativistic, neutrinos can be formed through the interaction between a proton and a gamma photon (Bethe-Heitler pair production) or the interaction between two protons. So, we discuss neutrino production and briefly how to estimate their flux. Finally, we talk about the detection methods and the detection through neutrino telescopes, in particular the high-energy events registered by IceCube Neutrino Observatory in 2018 from the blazar TXS 0506+056 and in 2022 from the Seyfert 2 galaxy NGC 1068.

Contents

Chapter 1

Introduction

Active Galactic Nuclei (AGN) are a class of extragalactic objects that apparently include a large variety of components. Their name comes from the first observation of these objects, where the brightest part of the galaxy was seen to be a compact region of the central part; this was the first clue for understanding how they work. This high luminosity requires for its explanation the presence of other processes than nuclear fusion, that generically explain the luminosity of a star (and so of a galaxy), and also the explanation of the Spectral Energy Distribution (SED) requires the presence of an "unconventional" process. These processes are all powered by the presence of a supermassive black hole (SMBH) in the center of every AGN, in which gravitational potential energy is converted into luminosity. The two main unconventional processes that happen in AGN are synchrotron radiation and Inverse Compton (IC), but for now, we postpone this discussion in chapter **3**.

These objects emit from the radio to the X-ray/γ-ray band of the electromagnetic spectrum, and are so bright that they have been observed at very large spatiotemporal distances; for this reason, they are a very important source for observational cosmology, in particular for the cosmological models of the evolution of the universe in its first billion years of life. For example, the proof of the isotropy of our universe for the $\sim Mpc$ distance scale was proved thanks to AGN.

At first, apparently different objects were classified as AGN, dividing them into categories based on the spectral characteristics observed. Therefore it seemed that it was a very heterogeneous class, united only by the presence of a very bright central part. Today, after about 70 years of studying these objects, we are very confident in dividing the AGN into two main categories: the *jetted* or *radio-loud* ones, and the *radio-quiet* ones.

1.1 Generic Structure

As mentioned before, in the center of an AGN there is a SMBH typically of $10^6 - 10^9$ $M_\odot$. The gas orbiting around this gain angular momentum and arrange in a plane, forming the accretion disk. In this, friction heats up the gas at high temperatures, forming a thermal spectrum that has the black body's peak in the optical-UV. Beyond the accretion disk, there is a torus (or a similar distribution; see [43], [33] and [32]) of gas, that has a high optical depth and so is one of the responsible for the heterogeneous appearance of the AGN. This appears obvious by looking the figure 1.1: depending on the line of sight, an AGN can appear very different.

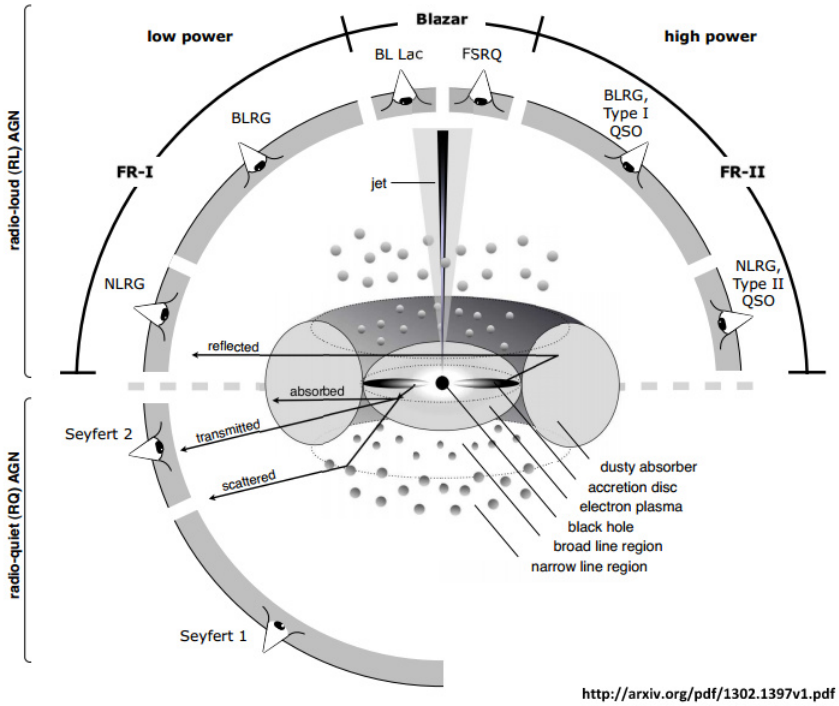

Figure 1.1: Schematic structure of the two types of AGN. The dashed grey line divides the two radio categories.

In addition to these components, considering the plane of the accretion disk as a symmetry plane, there are two regions of gas that form emission lines in the optical and UV: the Narrow Line Region (NLR) and the Broad Line Region (BLR). The NLR is located further out and there the gas moves slower with respect to the other region. The BLR, having the higher velocity gas, has broader lines; the velocity is probably radiated driven by the accretion disk. The NLR, combining the slower velocity and the lower densities of the gas, has narrower lines.

Around the SMBH most likely there is a hot corona that contributes to the X-ray continuum. This structure is assumed to be in spherical geometry and is formed mainly by relativistic electrons and protons; the geometry is supported by the Compton reflection observed in some sources, see [35]

The main difference between radio-quiet and jetted AGN is, as the name suggests, the presence of a jet and its activity in the radio part of the spectrum; also the jets are responsible for the heterogeneous appearance of the AGN. In these structures, plasma is ejected with high velocity, relativistically at least in the first part of the jet. Observationally, the difference between the two radio classes is measured by the ratio of the flux in two specific frequencies, for example, measuring the flux in the B band (F_B), and the flux at 5 GHz (F_5). Based on [29], we talk about a jetted AGN when:

$$F_B/F_5 \gtrsim 10$$

Looking at the figure 1.2 on the following page, the reason for this selection method is clear: the gap between the radio-loud and the radio-quiet at 10 GHz is almost two

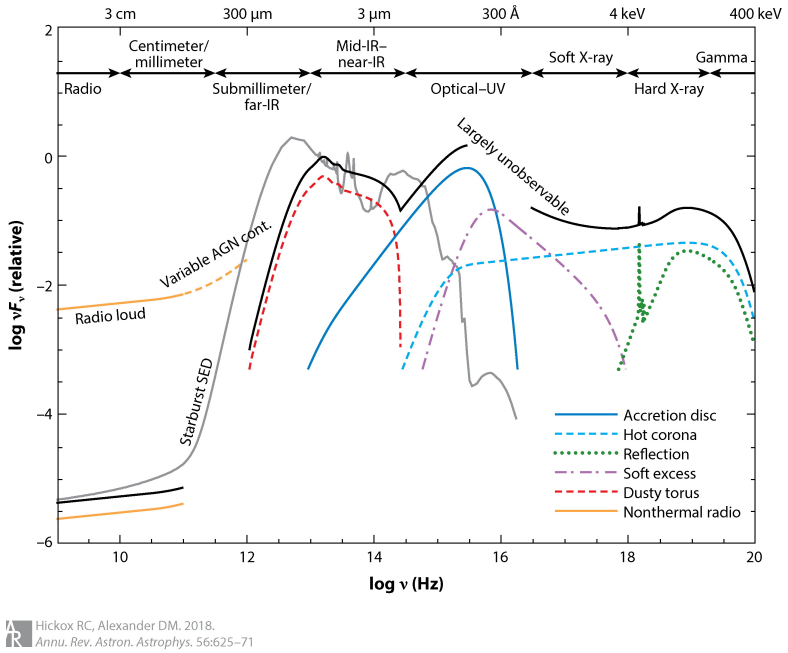

Figure 1.2: There can be seen the difference between a radio-quiet AGN (black) and a star-forming galaxy (grey). It clearly appears that AGNs have a substantial emission for all the electromagnetic spectrum.

orders of magnitude. The overall plot refers to a radio-quiet AGN; in the chapter **3** there is a comparison with a blazar SED. We note that the thermal radiation of the torus and the accretion disk dominates respectively the infrared and the optical-UV of the SED, while the corona largely contributes at higher energy together with other processes that vary according to the type of AGN.

Based on that, roughly $15-20\%$ of AGNs are jetted. These have two jets, roughly symmetric with respect to the plane of the accretion disk, in which particles are accelerated by the electromagnetic field generated by the SMBH. Based on what particle is accelerated, it forms a specific radiation output. Electrons form synchrotron radiation that is responsible for the smooth non-thermal radio radiation that characterizes this class of AGNs; part of synchrotron photons are also the main source for the IC. Protons, if relativistic, take part in more complex processes, that at the end form γ-ray and high-energy neutrinos, typically in the order of TeV or even PeV. Due to this, jets are the principal source of the radio and γ-ray part of the SED, and also for neutrinos.

In the figure 1.1 on the previous page are summarized the main structures of the 2 AGN categories; the names surrounding the image refer to their classification, which is discussed in chapter **2**. To contextualize, a 10^8 $M_\odot$ black hole has a Schwarzschild radius[1] of ~ 6 AU, from ~ 10 to 10^3 UA begin the accretion disk, BLRs are located

[1]This is a radius r_g associated with every mass M, which coincides with the event horizon of a Schwarschild black hole (spherical, non-rotating and without electric charge). It correstpond to:

$$r_g = \frac{2GM}{c^2}$$

where G it's the universal gravitational constant.

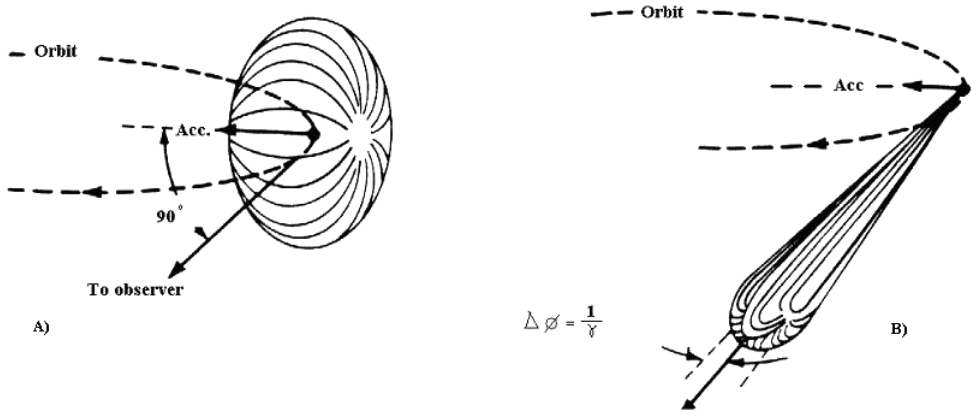

Figure 1.3: Angular distribution of a charged particle in the classical case (left) and relativistic case (right). Note that $\Delta\phi$ is the aperture of the radiation cone, and depends on the inverse of the γ factor of the particle.

within $\sim 10^{-2}$ pc of the black hole and NLRs extend from ~ 1 to 10^2 pc. The dusty torus begins at $\sim 10^{-1}$ pc, and jets begin within this scale and may produce radio-emitting structures extended up to $\sim$ Mpc scale.

1.2 Evidence of relativistic jets

The two principal phenomena that suggest the presence of a relativistic component in the AGN have already been mentioned above:

- **"Extreme" brightness temperature**. Jetted AGN have temperature $T \gtrsim 10^{10}\ erg\ s^{-1}$ and this temperature is too high to be due to thermal processes.
- **Synchrotron radiation**. This radiation occurs when charged particles move relativistically in a region permeated by a magnetic field. The particles form a curved path, and the result is radiation collimated along the velocity vector (see figure 1.3); the collimation and the peak of the radiation are greater the closer particles get to the speed of light. So, since we are sure that the lower-energy radiation of the SED is explained like this, there is some process that accelerates particles at relativistic energies.

As introduced in [13], the presence of a relativistic component in the jet forms different phenomena: rapid variability in the spectrum, high polarization, high luminosity, and apparent superluminal transverse velocity[2]. These are a direct consequence of the special relativity effect of the transformation of angles (relativistic aberration), and when we see these peculiarities in an AGN, we are almost completely sure that there is a relativistic component. To understand these effects it's important to introduce the *Doppler factor*:

$$\delta = [\gamma(1 - \beta\cos(\theta)]^{-1} \tag{1.1}$$

[2]This occurs when the angle between the line of sight and the velocity vector of the source is small.

where $\beta = v/c$ is the velocity of the source (respect a generic reference frame) related to the speed of light, $\gamma = 1/\sqrt{1-\beta^2}$ is the respective Lorentz factor and θ is the angle between the velocity vector and the line of sight of the observer (generically lay in the reference frame in which velocity is measured). This factor becomes strongly important when the speed of the source becomes relativistic: in the case that the line of sight is aligned with the velocity vector ($\theta = 0$), the δ tends to ∞ when β tends to unity. With this equation, we can explain the mentioned phenomena that we see in the jets:

- **Superluminal motion**. While emitting photons, a relativistic source "runs after" these. So, if the line of sight forms a small angle with the velocity vector [30] of the source (θ tend to 0 in equation (1.1)), in the observer frame the observed time interval, Δt, differs from the intrinsic one, $\Delta t^{'}$:

$$\Delta t = \delta^{-1} \Delta t^{'} \tag{1.2}$$

  So, when we calculate the transverse velocity of the source, we overestimate this because the perceived time interval is shorter. Typically values of superluminal motion are in the order of $\sim 30\mathrm{c}/(\mathrm{H}_0/50)$ [46];

- **Enhancement of luminosity**. Inverting the relation in the previous point, we found an analogous relation for the perceived frequencies, ν, in relation to the intrinsic one, $\nu^{'}$:

$$\nu = \delta \ \nu^{'} \tag{1.3}$$

  it follows that we receive blue-shifted (neglecting the motion of the source with respect to the observer) radiation. If we calculate the specific intensity ($I_\nu(\nu)$), we find that there is a boosting in this one respect to the original one ($I^{'}_{\nu'}(\nu^{'})$):

$$I_\nu(\nu) = \delta^3 I^{'}_{\nu'}(\nu^{'})$$

  Integrating over frequencies, there is an another δ factor due to (1.3):

$$F = \delta^4 F' \tag{1.4}$$

  and so will be for the luminosity;

- **High variability**. The degree of variability in AGN is frequently measured by the change in flux over time, substantially a relative change in flux about $> 30\%$. From equations (1.4) and (1.2) we obtain:

$$\frac{F}{\Delta t} = \delta^5 \frac{F'}{\Delta t'} \tag{1.5}$$

  Several AGN are seen in the condition to observe this phenomena (they are called *Blazar*), and the time-scale of variability is in the order of a few days.[3]

- **High polarization**. Synchrotron radiation is particularly efficient for lighter particles, so are generically the electrons the ones that power that. Generically, in the jet, electrons have a helical motion, and we know that when a charged

[3]The equations of the previous two points are valid for a point-like source, but in our case, we can't make this assumption. The consequence is a decreasing of a δ in the equation, due to Lorentz length contraction.

particle moves in a not uniform motion it emits radiation. This is polarized in parallel to the acceleration vector, that is in the plane perpendicular to the magnetic field. The polarization depends on the orientation and the variation of the magnetic field.

Another evidence of the presence of relativistic jets comes from the presence of the γ-ray radiation. In order for these high-energy photons to escape the source, the optical depth at these wavelengths must be of order unity or less; this is equivalent to saying that *compactness* must be less by 40. This dimensionless parameter is proportional to the ratio of luminosity-dimension of the source:

$$\ell = \frac{L}{r} \frac{\sigma_T}{m_e \, c^3} \tag{1.6}$$

where L is the luminosity and r is the dimension of the source, m_e is the mass of the electron and σ_T is the Thomson cross-section.

If we calculate this with the apparent luminosity of an AGN, it is in order of $10^3 - 10^4$, so the γ-ray luminosity must be much smaller than the observed one. This is resolvable if we assume a relativistic motion, using an analogous (1.4) equation to put the intrinsic luminosity in the compactness equation; so an additional δ^{-4} factor will appear, and the compactness can easily become smaller.[4] From equation (1.6), knowing the observed luminosity and using the mentioned constraint, we can also estimate the Doppler factor. The values of the δ factor change from object to object, but it is always > 1.

[4] An additional δ factor will come from the estimation of the dimension r, that is proportional to the variability time scale.

Chapter 2

Classification

In the following chapter, we briefly discuss the empirical and a schematic classification, which is part of the *Unified schemes*. As the name suggests, in these schemes we try to classify together objects that are apparently heterogeneous, but they are substantially the same ones observed in different ways.

2.1 Empirical classification

As we mentioned before, if we see an AGN spectrum that has an approximately smooth and strong radio component, we talk about jetted AGN. The other parts of the spectrum of the two radio classes are similar, suggesting that they have similar processes that form radiation in these spectral domains [43]. Furthermore, there is a correlation between jetted ones and black holes spin ([2] and [12]), host galaxy type [44] and γ radiation, that is jetted ones are located in luminous elliptical galaxies, have a spinning SMBH and have a considerable γ radiation. All these differences that are found in observing AGNs are intuitively useful for making a systematic classification.

So when was observed the first handful of AGNs, approximately in the '60s, they began to be classified according to similar characteristics, as has been done with the stellar spectra or with atomic elements. Unfortunately, unlike the two mentioned examples, this way of classification turned out to be messy: dividing the AGNs in this way forms very different classes, due to their "anisotropic" structures. Unfortunately, if we classify them in this way we are not "extracting" the physics of these objects, as it happened with stellar spectra classification and the periodic table.

Anyway, this classification forms generically three broad types that contain both radio-loud and jetted ones:

- **Type 1**. These have bright continua and broad emission lines from hot, high-velocity gas. The radio-quiet are called Seyfert 1 galaxies and radio-quiet quasars that are respectively lower and higher luminosity ones. For the jetted ones, we have Broad-Line Radio Galaxies (BLRG) at low luminosity and radio-loud quasars at high luminosity, divided into Steep Spectrum Radio Quasars (SSRQ) or Flat Spectrum Radio Quasars (FSRQ) depending on radio continuum shape;[1]

[1]Quasars are apparently point-like objects seen at the higher distances, and radio galaxies are located nearly and spatially resolved.

- **Type 2**. These have weak continua and only narrow emission lines, meaning either that they have lower velocity gas or, as we see later, the line of sight to high-velocity ones is obscured by the dusty torus. Radio-quiet are Seyfert 2 galaxies at low luminosity, while the high-luminosity counterparts don't have a clearly identified subclass. The jetted ones are called Narrow-Line Radio Galaxies (NLRG) and are divided into Fanaroff-Riley I (FRI) and the Faranoff-Riley II (FRII) [24]. The first ones have lower luminosity, two-sided jets, and distorted lobes, while the others have often one-sided, more collimated jets, higher luminosity, and two radio lobes (called hot spots). These differences come from the presence of a more efficient radiative transport mechanism in the FRII, that causes a powerful jet with prominent relativistic motion, responsible for the one sided-jet due to relativistic aberration. This can be seen in the figure 2.1. FRIs probably have relativistic jets too, but at a lower distance scale;

- **Type 0**.We call them in that way following [45]. AGNs with unusual spectra are classified there. These include the BL Lacertae (BL Lac) objects, which are jetted AGNs that lack strong emission or absorption lines. There are also many subclasses of objects that we can classify in there, which include also some FSRQ. They have in common high variability, high and variable polarization, and high brightness temperature; these are all evidence of relativistic motion, as seen in section 1.2. They have also continuum spectra that resemble the BL Lac ones. Due to these high variable characteristics, we think that they are more or less the same objects, so they are referred to simply as FSRQ. Together with BL Lac, we call them Blazars.

Note that we mentioned only the main AGNs subclasses, and thus already is a confusing empirical classification.

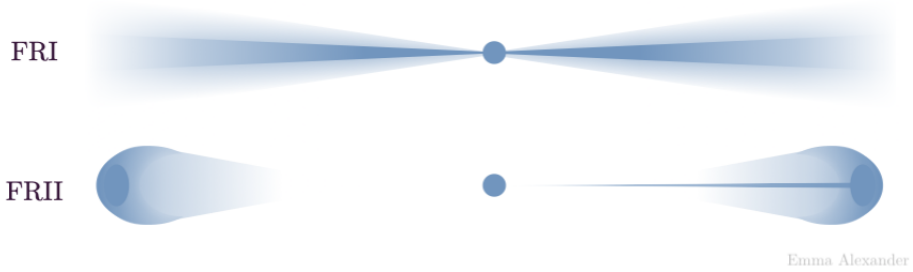

Figure 2.1: Schematization of the visual differences between the two FR classes. In practice, the FRI doesn't have straight lobes, and FRII doesn't have hot spots of the same shape. For FRII, the jet sided to the observer is collimated and boosted in the direction of relativistic motion; the same for the counter-jet, but in the opposite direction. This causes the one-sided view. Image credit: Emma Alexander - [1], CC BY 4.0, Wikipedia.

The only thing that we can "extract" from this classification is not an intrinsic physical one, but a spatial-distribution one, as we can see in figure 1.1: the *angle of view* decrease with the Type number. This angle is measured as the angle between the line of sight and the symmetry axe of the AGN (that is, for radio-loud, roughly the jet axe), and can vary from 0° to 90°. To be more specific Type 0 are seen near 0°, Type

2 near 90°, and Type 1 at middle angles. Since Type 1 are seen at middle angles, we can see the NLR, BLR, and also the radiation from the center of the AGN; in fact, we see broad lines from BLR and a strong continuum from the central region. The Type 2 have higher angles, so the dusty torus absorbs the radiation of the central region, and we see only the NRL and the radiation from the jet. Lastly, Type 0 have smaller angles, so only the radio lobes of jetted ones or the polar outflow of the radio-quiet are seen.

We can conclude that in this empirical classification, Type 1 or 2 depends on the obscuring torus and Type 0 depends on the alignment of the line of sight with the jet/outflow axes. Beyond this, we cannot say anything else and intuitively we cannot with any of these ways to classify.

2.2 Unification schemes

If the complex structure is a problem for an intuitive classification, it turns out that is the clue for a simplest one. First of all, it is worth to analyze the causes of anisotropy.

The obscuration by the dusty torus is supported by the observations. In particular, the detection of polarized light from the central region of Type 2 AGN has been associated with the obscuration by the torus. The spectrum of polarized radiation shows broad emission lines very similar to the Type 1 objects, supporting the fact that, at a large viewing angle, the photons from BLR and the central region are absorbed by a distribution of gas or dust; polarization is caused when the radiation is scattered toward the observer. Observing broad lines in the infrared spectra of Type 2 AGN, where optical depth is smaller, confirms the presence of a central obscured region. Also, the weakness of the X-ray continuum of the Type 2 objects is explained by the presence of the torus (see [1], [22] and [23]). Another evidence of obscuration comes from optical images.

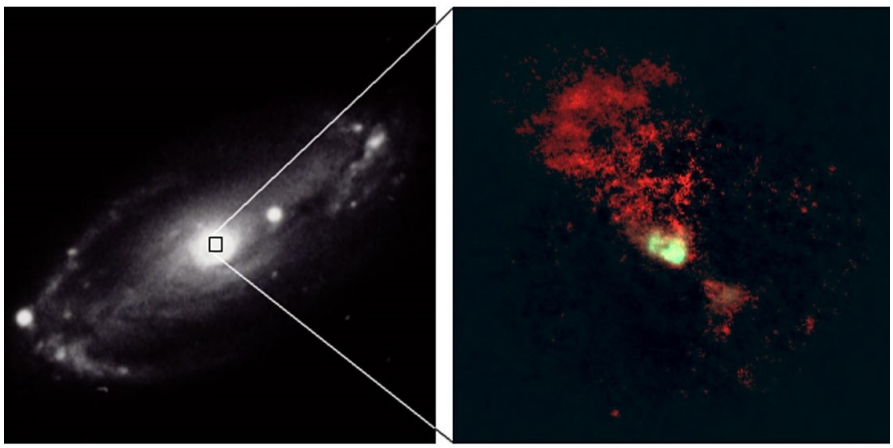

Figure 2.2: Two different visions of NGC 5728, that is a Seyfert 2 galaxy. The apex of the structure coincides with the position of the obscured nucleus.

The biconical structure in figure 2.2 is evident and indicates that the AGN radiation that is photoionizing the NLR is not illuminating the gas in an isotropic way.

Another fact is that Blazars have higher superluminal velocities (see [27] and [46]) in agreement with the idea that their jets are more aligned with the line of sight than other classes of jetted AGN. For this category we note that both FRI and FRII radio galaxies have pairs of jets, so we can conclude that they are only misoriented Blazars. In addition to the differences mentioned in the previous section, Fanaroff and Riley note that FRI types tend to have weaker optical lines (see [38], [42] and [20]) than FRIIs, and tend to inhabit relatively rich cluster environments (see [36] and [25]) than FRIIs. Considering all these things, one can intuitively conclude that the FRIIs are the "powerful"[2] counterpart of the FRIs.

So, the presence of the torus and the jets can be used to make two simple Unification Models, based on the previous evidence/assumption. The two models that we will see below are simplifications of reality, so they are valid in general but don't always work perfectly.

2.2.1 Unification of jetted AGN

It is widely accepted that jetted AGNs are the same object seen at a different angle of view due to the orientation of the relativistic jet. The FRI and FRII are instead unified on the basis of jet power. Following Urry and Padovani [45] we can ideally associate the jetted AGN with a single, power radio-loud source observed at different viewing angles. The appearance of the object changes from the one of a Blazar (core-dominated in the radio; weak and or/polarized broad emission lines in the optical), to the one of type 1 FRI and FRII depending on radio luminosity, and to the one a type 2 at large viewing angle (see figure 1.1 on page 4).

The luminosity of FRII and quasar narrow lines are comparable, and observing both objects in the infrared it is noted that these are more luminous, confirming the presence of an obscuring torus. Studying their host galaxies morphology type it's difficult because these objects are located principally at high redshifts; despite that, they see that these galaxies are both probably luminous ellipticals.

FRI and BL Lac are located at lower redshifts, so it was easier to resolve them; it was discovered that both are giant ellipticals. Also their cosmic evolution is similar and it was seen that they are located in a similar environment, that is clusters rich in galaxies.

2.2.2 Unification of radio-quiet AGN

Similar studies were made to unify radio-quiet, with the result that Seyfert 1 and Seyfert 2 are the same objects. In particular, in [37] it was seen that a Seyfert 2 galaxy, NGC 1068, has BLR polarized lines in his spectra, suggesting the presence of an absorbing structure that "covers" the BLR region in the center. Note that this is in agreement with the affirmations in the caption of figure 2.2: in this, we have a Seyfert 2 galaxy, and indeed we indirectly see the obscuring torus. Lastly, radio-quiet AGNs are generically located in spiral galaxies. All of this suggests that they are the same object, that appears either of Type 1 or Type 2 due to the obscuring effect of the torus.

[2]Here "powerful" means that the extraction of energy from the SMBH is more efficient.

Chapter 3

Models for Jetted AGN

There are many open questions in the explaining of the formation and the dynamics of relativistic jets, which are about: the primary physical mechanism powering the jet, the strength and topology of magnetic fields along the jets, the plasma components, and consequently the dominant radiative output that we see in the SED. In the following chapter, we explain the basic ingredients for a general jet model and then discuss the two main types of these, which differ according to their relativistic composition: *leptonic models* have only electrons and positrons and *hadronic models* have also protons. The latter are the less accredited models because they have a higher number of free parameters and the SED of an AGN can also be explained without an hadronic relativistic component. In addition, we know that protons are approximately 10^3 heavier than electrons, so they are more difficult to bring at relativistic energies and thus the system needs to have an overall higher energy.

So, why do we want to talk more about these models? As mentioned in the introduction and as we will see in section 3.3, these are the models that can form TeV or even PeV neutrinos. We will also see in the next chapter that observational evidence confirms that these models are destined to become more important in the future of the study of jetted AGN.

So it is obvious that from now we focus the discussion only on the jetted AGN, ideally on the FRIIs; as said in the paragraph 2.1 these have powerful jets. Since neutrinos form at high energies, and in particular they are associated with high-energy radiation, it is appropriate to restrict our discussion to powerful AGNs.

It is important to say that the next section is based on [40].

3.1 Fundamental basis for jet models

A jet phenomenon appears to be common wherever mass accretion onto a central object occurs, and becomes relativistic in the case of accretion onto compact objects. In our case the compact object is an SMBH, which forms a large-scale jet, but small-scale ones can form from neutron stars or smaller black holes. Although we don't know the exact physical mechanism that occurs, it is known that the jet components come from the accretion disk of the SMBH. More specifically, the inner part of the disk forms the coronal plasma that surrounds the black hole, and this is evacuated by magnetocentrifugal effects to form a bipolar jet.

3.1.1 Geometry

It is thought from [39] that the jets formed at a distance z_0 from the black hole, and hence from that can be treated as a distinct physical component; this parameter is the characteristic scale of the coronal plasma. The geometry of the jet strongly depends on the proprieties of the components when are accelerated, but there is evidence, discussed in [8] and [34], for M87 that the base of the jet has approximately a paraboloidal shape which become conical at higher distance scale. This is consistent with the predictions of a collimated, magnetically-dominated flow that is converted to a kinetically dominated flow. At distances $\gg 10^5 r_g$, where r_g is the Schwarzschild radius of the SMHB, jets appear to be well collimated in a quasi-cylindrical structure; it is often adopted to assume that jet has this structure all along the section responsible of the radiative output. Despite that, it is more correct to consider the jet a conical structure, whose cross-sectional radius is parameterized as:

$$r(z) = r_0 \left(\frac{z}{z_0} \right) \tag{3.1}$$

where z is the distance from the center of the SMBH, as we see in the figure 3.1 on page 16. In this, the green region represents the accelerating region, and z_{end} parameterizes the end of the jet.

3.1.2 Emitting region

The emission of high-energy and very-high-energy γ-rays requires the acceleration of particles to TeV or even PeV energies. This is possible only in relatively small regions along the jet and due to the short cooling time scale of the particles, we expected to see the radiation mentioned before. Combining this with the observed rapid variability of the jets, models can consider the emitting region formed only by a single, homogeneous region (assumed spherical for simplicity) in which there are uniform physical conditions. These assumptions are obviously simplifications but are popular due to their relative simplicity. In [26] is pointed out that models must consider a multi-zone emitting region, which is necessary for a consistent model. However, this causes an increase of free parameters and these models are not yet self-consistent with the magnetohydrodynamics[1] (MHD).

3.1.3 Energetics

In the following discussion, we parameterize the energetic extraction from the SMBH to the relativistic particles by defining different types of luminosity; here the luminosity is defined as the variation of the energy with respect to time and q_i are all dimensionless parameters (where the subscript i will be an abbreviation) with different physical meanings.

The accretion power of an SMBH of mass M_{BH}, parameterized by its Eddington luminosity L_{Edd}[2], it is expressed through the mass accretion rate $\dot{M}$:

[1] This is the discipline that studies the dynamics of the charged fluids. In our case, it is important to describe the structure formed by the plasma in the jet.

[2] This is the maximum luminosity that a body can have remaining in hydrostatic equilibrium. It can be expressed in term of the mass M of that body:

$$L_{Edd} = 3.2 \times 10^4 \left(\frac{M}{\mathrm{M}_\odot} \right) \mathrm{L}_\odot$$

$$L_{accr} \equiv \epsilon \dot{M} c^2 = q_{accr} L_{Edd} \approx 1.3 \times 10^{46} q_{accr} \left(\frac{M_{BH}}{10^8 \ \mathrm{M}_\odot} \right) \mathrm{erg} s^{-1} \tag{3.2}$$

where ϵ is an efficiency dimensionless parameter, that tells us the portion of the gas that fell in the SMBH that is converted in energy (and so in luminosity). For an accretion disk, this is $\epsilon \sim 0.07$. The introduced parameter q_{acc} is the ratio between the luminosity of the accretion power of the SMBH and the Eddington luminosity.

A fraction of this is ejected in two symmetrical jets, each carrying:

$$L_{jet} = \frac{1}{2} \ q_{jet} L_{accr} \tag{3.3}$$

where $q_{jet} < 1$; this parameter is the fraction between the luminosity of the jet and half of the luminosity in equation 3.2. The presence of the $\frac{1}{2}$ factor implicitly assumes that L_{accr} is divided symmetrically between the two jets. The equation also assumes the mechanism discussed in [10], thus if enhancement from the black hole spin is relevant (see [11]) this linear relationship with the accretion disk luminosity may no longer hold.

As we said, the injection of particles from the corona to the jets is driven by the magnetic field. To allow this, the magnetic energy density at the basis of the jet must be enough to reach the kinetic energy that the jet plasma achieves. So the energetic densities at the basis must stand at the condition of equipartition:

$$U_{mag}(z_0) \geq U_{kin}(z_0)$$

In the most accepted models, part of the magnetic energy is converted into kinetic energy of the plasma, bringing the bulk Lorentz factor, Γ_{jet}, to a maximal value. The region in which this occurs can be seen in green in figure 3.1.

There are two possible mechanisms for the acceleration: diffusive shock acceleration (DSA) or fast magnetic reconnection in the presence of turbulence. In the first case the plasma gain kinetic energy because they get repeatedly reflected, for example for a magnetic mirror; the second mechanism works better for jets with high magnetization, in which the acceleration comes from the fast variation of the topology of the magnetic field. In both cases, to calculate the maximum energy reached by the particles in the plasma, we have to equate the total energy-loss rate (see the next section) with the acceleration rate:

$$\left. \frac{\mathrm{d}E}{\mathrm{d}t} \right|_{acc} = - \left. \frac{\mathrm{d}E}{\mathrm{d}t} \right|_{tot} \tag{3.4}$$

the right member represents a loss of energy, so we must put a minus sign. Following [21], a simply acceleration rate is proportional to the magnetic field:

$$\left. \frac{\mathrm{d}E}{\mathrm{d}t} \right|_{acc} \propto B(z) \tag{3.5}$$

We parameterize the power transferred to the relativistic plasma as:

$$L_{rel} = \ q_{rel} L_{jet} = L_p + L_e = (1 + a) L_e \tag{3.6}$$

where also here $q_{rel} < 1$, and this parameter represents the fraction of jet luminosity that is converted into relativistic luminosity. The subscripts p and e stand respectively for protons and electrons. The parameter a comes from $L_p = a L_e$, so it parameterizes the proton's luminosity as a function of the electrons. This is useful to distinguish the leptonic models, where $a < 1$, from the lepto-hadronic ones, where $a > 1$.

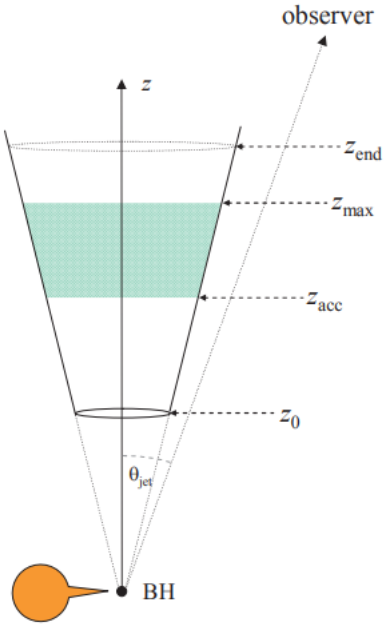

Figure 3.1: Simplified geometry of a jet. θ_{jet} is the angle between the observer and the z axis.

3.1.4 Microphysics of the component of the jet

The most important interaction between the magnetic field and the particles of the jet is synchrotron radiation. For a charged particle of mass m, energy $E = \gamma mc^2$ and charge $q = Ze$, the synchrotron energy-loss rate is (e.g., [14]):

$$\left.\frac{\mathrm{d}\gamma}{\mathrm{d}t}\right|_{synch} = -\frac{4}{3}\left(\frac{m_e}{m}\right)^3 \frac{c\,\sigma_T\,U_{mag}}{m_e c^2}\,Z^4\gamma^2 \tag{3.7}$$

where m_e is the electron mass, σ_T is the Thomson cross-section, and U_{mag} is the magnetic energy density. We note that this cooling is much more efficient for lighter particles; for example, the process is approximately 10^{27} more efficient for electrons than for protons (assuming equal Lorentz factor and magnetic energy density).

The photon field generated from this process can interact with relativistic particles by IC scattering, forming a synchrotron-self-Compton (SSC) process; in the leptonic models this dominates the X-ray and also the γ-ray radiative output. The Compton effect occurs when a high-energy photon collides elastically with a particle, so the IC process is when the photon is hit by a relativistic particle. The IC can also happen through an external photon field, such as photons from NLR, BLR, accretion disk, and the torus (models that consider these scenarios are called External Compton models). The particle cooling for this mechanism has an analogous equation to the one above, except for replacing U_{mag} with U_{rad}, which is the energy density of the target photon field. This analogy makes that IC is considered only for light particles, except in the case of very high energy [6].

If a photon reaches the threshold energy of $\sim$ 1MeV in the proton rest frame, the

photopair described in the Bethe-Heitler process[3] takes place:

$$p + \gamma \rightarrow p + e^- + e^+ \tag{3.8}$$

At even higher energy of the photon ($\sim$ 145MeV always in the proton rest frame), takes place the *photomeson* process, with two channels that have the same cross-section:

$$p + \gamma \rightarrow p + a\pi^0 + b(\pi^+ + \pi^-) \tag{3.9}$$

$$p + \gamma \rightarrow n + \pi^+ + a\pi^0 + b(\pi^+ + \pi^-) \tag{3.10}$$

where a and b are integers and represent the pion multiplicities. We can call the two processes above as $p\gamma$ interactions. For completeness, the threshold energy of the proton in the laboratory frame is expressed as:

$$E_p^{thr} = \frac{m_p c^2 \; m_\pi c^2}{2 \; E^{ph}} \left(1 + \frac{m_\pi}{2m_p}\right) \sim 7 \times 10^{16} E_{\mathrm{eV}}^{-1} \text{ eV} \tag{3.11}$$

The energy-loss rate of the pγ interactions is very complex (see [9] for the complete calculus); in synthesis, it depends proportionally on the photon distribution, the cross-section, and the inelasticity of the process (the fraction of the proton energy lost per interaction), and it is inversely related by the Lorentz factor of the proton. In [9] there are two analytical expressions, using a power-law and a blackbody spectrum for the photon distribution. These distributions play an important role in the subsequent protons energy distribution and so in the energy distributions of the secondary particles (the ones that are formed by interaction between particles injected in the jet). In general, the photon distribution has to consider all the photon fields produced internally and externally to the jet, but we can make simplifications depending on the model considered.

The charged pions rapidly decay in leptons and neutrinos:

$$\pi^+ \rightarrow \mu^+ + \nu_\mu, \quad \mu^+ \rightarrow e^+ + \nu_e + \bar{\nu}_\mu \tag{3.12}$$

$$\pi^- \rightarrow \mu^- + \bar{\nu}_\mu, \quad \mu^- \rightarrow e^- + \bar{\nu}_e + \nu_\mu \tag{3.13}$$

whereas neutral pions decay in:

$$\pi^0 \rightarrow \gamma + \gamma \tag{3.14}$$

Neutron from equation 3.10 can also decay by the *negative β decay*:

$$n \rightarrow p + e + \bar{\nu}_e \tag{3.15}$$

This reaction typically takes place outside the jet, due to the charge neutrality of the neutrons and for the relatively high mean lifetime ($\sim$ 15 minutes in the term of neutron proper time[4]). Charge neutrality allows them to escape from the electromagnetic confinement of the jet, so the external decay allows neutrons to be a candidate

[3]This is a type of pair-production that concerns a proton and a photon. Since the pair-production concerns the creation of a subatomic particle and its antiparticle from a neutral boson, in this case the proton can be seen as a catalyst.

[4]The proper time of an object is the time calculated in the object rest frame.

source for high-energy cosmic rays. The β decay is also important for the discovery of the neutrino; for this and further information about neutrinos see appendix A.

So, only 3.12 and 3.13 are the reactions that produce neutrinos inside the AGN; note that all these decays refer to their dominant channels (in both charged and neutral pion decay, in $\sim 99\%$ of the cases are formed those products). Models that consider pγ productions require a magnetic field $\gtrsim 10 - 100G$. In this situation, the dominant photon field is the one that comes from the synchrotron radiation by the primary electrons (the one that does not come from the decays) of the jet, so we can consider that field for the IC.

Jets are usually a low-density place, but in the case of a denser jet, one can consider the proton-proton interaction. Indeed, if these interactions take place they must be considered for proton cooling and for the radiative output. They interact similarly to the processes above, forming charged and neutral pions, that inject photons and leptons in the system. From [9], the energy-loss rate for a proton of energy E that goes through this process is:

$$\left.\frac{\mathrm{d}E}{\mathrm{d}t}\right|_{pp} = -n_p \; c \; E \; \kappa_{pp}\sigma_{pp} \tag{3.16}$$

where e n_p is the number density of protons in the *co-moving* frame (the frame fixed with the jet plasma) σ_{pp} is the proton-proton cross-section, and κ_{pp} is the inelasticity of the interaction, that is ~ 0.5.

Another process that contributes to the cooling of the plasma jet is adiabatic cooling, which depends on the jet geometry (and so on the position of the plasma along the jet). In general, is:

$$\left.\frac{\mathrm{d}E}{\mathrm{d}t}\right|_{ad} = -\frac{E}{3}\frac{\mathrm{d}V}{\mathrm{d}t} \tag{3.17}$$

The total energy-loss rate that appears in equation 3.4 is simply the sum of all the prevalent cooling processes.

Finally, the particle distribution can be expressed by a complex transport equation, that can be simplified based on the models. This equation consider: the variation of particle number along the time, particle convection along the jet, energy losses/gains, decays, and escape of particles.

3.1.5 Non-thermal radiative output

The dominant radiation mechanisms from the accelerated particles are: synchrotron radiation (of primary electrons and protons and secondary pions, muons, and electrons/positrons), IC scattering (relevant only for electrons and positrons), and π_0 decay. Some simplified equations (calculated in the co-moving frame) for all three are found in [40]. For us, it's important to keep in mind that synchrotron radiation and IC depend on the particle's energy distribution, whereas π_0 decay depends on the cross-section of the pγ interactions, the inelasticity and the branching ratio (the fraction of neutral pion production).

Furthermore, there are two corrections that can be made: electron that can absorb the radio frequencies photons (Synchrotron-Self absorption, SSA, see [41] and [15]) and photon-photon annihilation that happens at high energies. In the latter, two γ photons can form electron-positron pairs.

Last but not least, from the pion decay we have electron and muon neutrinos that can be produced if the threshold energy is reached. In the next chapter, we will see that there has been evidence in recent years of neutrino emission from two AGNs.

In figure 3.2 we see a typical SED of a blazar, with his "double-humped" shape; the left peak corresponds to the synchrotron radiation and the right one corresponds to the higher energetic processes (which vary according to the model). There is also the predicted neutrino flux of the source and the IceCube event (the red cross) which is thought to be linked with that blazar. The low energy peak is well explained with the synchrotron radiation, while the high energy peak is still debated.

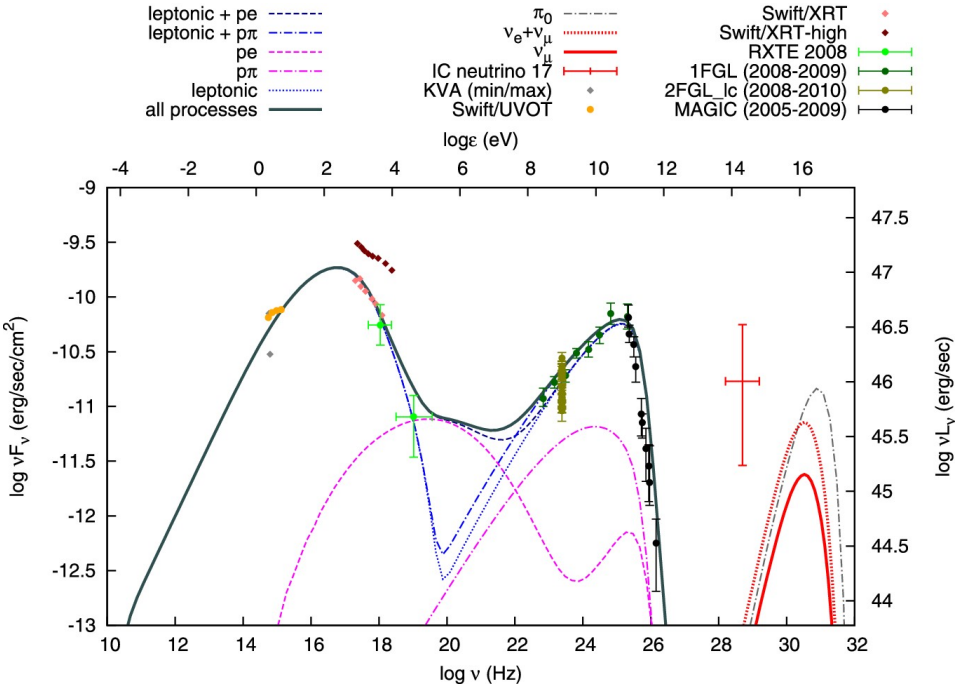

Figure 3.2: SED of blazar H 1914-194 and the neutrino flux for the corresponding IceCube event (ID 22). The *pe* process is the photopair (3.8) and the $p\pi$ is the photomeson (3.9)-(3.10). Data are obtained from ASI Science Data Center. Image credit: [31].

3.2 Leptonic Model

The most popular class of models adopts the leptonic model, in which the high-energy component is the result of the IC scattering by the same electrons responsible for the synchrotron emission. Different sources of photons can be considered and obviously, the emission will be dominated by the photon field with the largest energy density (measured in the co-moving jet frame). The two generic scenarios, the SSC and the External Compton (EC), were briefly discussed in the sub-paragraph 3.1.4.

The SSC process dominates in the case of very weak or even absent thermal radiation from the center of the AGN, so regard SMBH that don't have a high accretion rate. A higher accretion rate corresponds to a bigger accretion disk and stronger ther-

mal radiation from the center of the AGN, which can also be reflected by the torus or the BLR. Following this reasoning, for the powerful AGN we can consider the EC process.

In these models, the jet also contains protons to ensure charge neutrality, but not at relativistic energies. In the absence of protons, we can assume a pure electron-positron plasma, always to ensure charge neutrality.

3.3 Lepto-Hadronic Model

To accelerate protons at relativistic speed, a strong magnetic field is required. For this reason, the lepton components of the jet emit through synchrotron radiation, so as the decay products. Jets densities are very low ($< 10^3 \mathrm{cm}^{-3}$), so the pion production processes are dominated by pγ interactions. In this case, the decay products are produced with Lorentz factors of $\gamma \gtrsim 10^7$, making possible the production of TeV or PeV neutrinos. The π_0 decay photons and synchrotron photons from electrons/positrons at these energies emerge beyond TeV energies. The emission region is highly opaque to these photons, so through pair production additional electron/positron pairs are produced in a cascading process. From equation 3.7 we note that the synchrotron cooling is highly efficient for lighter particles, so protons practically don't emit through this process. Considering that synchrotron cooling is the primary and the stronger cooling effect that happens when a particle becomes relativistic, if the magnetic field in the jet is strong enough, from equation 3.4 turns out that protons can be accelerated efficiently; consequentially the can overcome the threshold energies of the pγ interactions. A direct determination of that is difficult, but if a neutrino detection is linked with an AGN, we are sure that a lepto-hadronic model is required.

Calculating the neutrinos flux from an AGN jet is very difficult, but the classical method can be summarized like this:

1. First is estimated the energy distribution for the protons and the photons, once a specific model has assumed which is the target photon field for the interaction. Typically the energy distribution is in the form of a power law function combined with an exponential cutoff. The steepness and the cutoff vary from model to model and depend on the cooling time scale (for protons) and the radiation source (for photons). A generic example is:

$$N_i(E_i) \propto (E_i)^{-\alpha_i} \times exp\left(- \frac{E_i}{E_{i,max}} \right) \tag{3.18}$$

   The subscript i is generic, it could be p for protons, for example. The first term is the power law, where α_i is the steepness and the second is the exponential cutoff. The cutoff happens when $E_i > E_{i,max}$, so $E_{i,max}$ is the maximum energy that the subject i can reach.

2. Through the cross-section of the interaction, can be calculated an energetic distribution for the neutrinos.

3. Then the neutrino flux can be calculated and then can be converted in our cosmological epoch. To do this, one has to know the luminosity function of the source, that is the function that tells how the sources of this type evolve during the cosmological time, and his redshift. This is because the number and

the energy density of the neutrinos (but generically for any particles that travel through spacetime) aren't conserved, due to the expansion of the universe.

Chapter 4

Neutrino detection and evidence of extragalactic neutrinos

Neutrinos are very elusive particles, that interact only through gravitational and weak interaction. Due to their very low mass (see appendix A) and their charge neutrality, the gravitational interaction is too weak to be detected and they don't interact via the electromagnetic field. So we can detect them only with weak interaction. This singular behavior is what arouses interest in scientists: if neutrinos can travel spacetime practically unchanged, this means that they can carry precious unchanged information about the source in which they are produced. This is extremely useful for every astrophysical source, in particular for the most distant ones or in case other messenger channels (photons, for example) are not effective.

4.1 Detection of neutrinos

Despite their behavior, the weak interaction between neutrinos and matter rarely happens. The two channels in which this occurs are:

- **Neutral current**. These interactions are mediated by the Z boson, which doesn't have an electric charge. The exchange of that boson transfers momentum, spin, and energy, but leaves the interacting particles' quantum numbers (charge, flavor, baryon number, lepton number, etc.) unaffected. Since there is no exchange of electric charge, there is the adjective *neutral* in the name of this interaction. In the detector, the neutrino enters and then leaves after having transferred some of its energy and momentum to a target particle. If this is charged and lightweight (as an electron), it might be accelerated to a relativistic speed and consequently emit Cherenkov radiation[1]. All three neutrino flavors (see appendix A) can participate, regardless of the neutrino energy. However, no neutrino flavor information is left behind.
- **Charged current**. These interactions are mediated by the W boson, which can have a positive or negative electric charge. In this interaction, there is also

[1]This radiation is formed when a charged particle moves faster than the speed of light in a dispersive medium, while remaining below the limit of the speed of light in vacuum. Consequently, a radiation cone is left behind the particle, similar to what happens when an object exceeds the speed of sound in the atmosphere. The angle of that cone depends on the γLorentz factor of the particle and the threshold speed of this effect depends on the dispersive medium.

a transfer of electric charge, and so there is the adjective *charged* in the name. A high-energy neutrino transforms into its partner lepton (electron, muon, or tauon), which can be detected through Cherenkov radiation. Since electrons are the lighter leptons, the channel that forms them is the most common, but also muons can easily form. A detector that can distinguish among these leptons can reveal the flavor of the incident neutrino. Target particles can be neutrons or protons, for example.

Taking this into consideration, different detection methods have been developed over the years. Generically, detectors are built underground to suppress the cosmic rays, that interfere with the neutrino's revelation. Below there is a list of some of the most important ones.

Scintillators Scintillation detectors are made of materials that emit ultraviolet or visible radiation when they are exited from high-energy photons or particles. These detectors were important for the discovery of the first antineutrino by the Cowan–Reines neutrino experiment in 1956. In this two scintillation detectors were placed next to the water targets. Here, antineutrinos with an energy above the threshold of 1.8MeV caused charged current (an inverse beta decay) interactions with the protons in the water, producing positrons and neutrons. The resulting positrons annihilate with electrons, creating pairs of coincident photons that could be detected by the scintillation detectors. The neutrons were captured by cadmium nuclei, forming γ-rays of about 8MeV could be detected too.

Cherenkov detectors In these, a large volume of clear material such as water or ice is surrounded by light-sensitive photomultiplier tubes. They are devices that convert incident photons into electrical signals. Once Cherenkov radiation is formed by charged leptons, this is detected by the photomultiplier tubes and shows up as a characteristic ring-like pattern of activity in the array of detectors. The ring pattern represents the "shock-wave" radiation of the Cherenkov light. Neutrinos can interact with atomic nuclei to produce charged leptons which emit Cherenkov radiation, and the formed pattern can be used to understand direction, energy, and sometimes flavor information about incident neutrinos.

These detectors were used in the Kamiokande and also in his today's successor Super-Kamiokande. This series of neutrino telescopes is located in the Kamioka Observatory in Japan. Important discoveries and confirmations regarding neutrinos have occurred here, as the discovery, in 1987, of the first cosmic neutrino from supernova SN 1987A, the confirmation that neutrinos are massive particles (specifically the strong evidence and successive study of the neutrino oscillation) and the study of proton decay. The first two studies have won the Nobel prize: the first in 2002 for Raymond Davis Jr. and Masatoshi Koshiba "for pioneering contributions to astrophysics, and in particular for the detection of cosmic neutrinos"[2] and the second in 2015 for Takaaki Kajita and Arthur McDonald "for the discovery of neutrino oscillations which show that the neutrino has mass".

Since the neutrino flux incoming to Earth decreases with increasing energy, if we are interested in them the size of these neutrino detectors must increase too. Building kilometer-sized cube detectors underground covered by thousands of photomultipliers would be prohibitively expensive, so detection volumes of this magnitude can be

[2]This prize was divided with Riccardo Giacconi "for pioneering contributions to astrophysics, which led to the discovery of cosmic X-ray sources"

achieved by installing Cherenkov detector arrays deep inside already existing natural water or ice formations. Doing this brings some advantages: at first, hundreds of meters of water or ice partly protect the detector from atmospheric muons (that can directly or not, by decay, interfere with the revelation of extraterrestrial neutrinos) and secondly, these environments are transparent and dark, useful for detecting the faint Cherenkov light. Examples of these enormous detectors are: the ANTARES telescope (Astronomy with a Neutrino Telescope and Abyss environmental Research) and the next-generation KM3NeT (Cubic Kilometre Neutrino Telescope), both in the Mediterranean Sea, AMANDA (Antarctic Muon And Neutrino Detector Array) and his successor IceCube, both inside Antarctic glacial ice near the South Pole. IceCube was also made for the detection of neutrinos from the most powerful sources, having so far detected dozens of high-energy events. Two of these are most likely neutrinos produced by AGNs, as we see in the next section.

Radio detectors There are ground neutrino detectors, that use antennas to detect Cherenkov or Askaryan[3] radiation. RICE (Radio Ice Cherenkov Experiment) and ANITA (Antarctic Impulse Transient Antenna) are both in Antarctica and are made to detect high-energy neutrinos, so they potentially can detect cosmic neutrinos from sources such as AGNs.

4.1.1 IceCube, the South Pole Neutrino Observatory

IceCube is a cubic-kilometer particle detector made of Antarctic ice and located near the Amundsen-Scott South Pole Station. This neutrino observatory was built under a National Science Foundation (NSF) Major Research Equipment and Facilities Construction grant, with assistance from partner funding agencies around the world. Detectors develop between $\sim$ 1500m and $\sim$ 2500m under ancient polar ice, which is ice practically free of imperfections. The arrangement of the detectors can be seen in the figure 4.1. The range of the instrument is from GeV to hundreds of PeV and above, with the observation of cosmic neutrinos at energies approaching 10PeV.

The most common neutrino detection comes from atmosphere neutrinos, so if we want to discover the high-energy astrophysical ones, it is necessary to discard these common events. IceCube works 24/7, and a software selects the most interesting event, for example selecting the events from a specific portion of the sky or selecting high-energy events. This is made by the GCN/TAN network (the Gamma-Ray Burst Coordinates Network and the Transient Astronomy Network) that since 2013 "alert" within seconds or minutes in the case of a particular situation. For our interest, there are two types of alerts (see GCN/TAN network for more details):

- **IceCube HESE** alerts announce the detection of a single high-energy neutrino that interacts inside the instrumented volume of ice. Uncertainty of muon neutrinos has a typical error of 1.5°. The pointing resolution for electron and tau neutrinos is very high, around 10°. The frequency of these alerts is three to four times per year. The first alert was sent in April 2016.
- **IceCube EHE** alerts announce the detection of a single extremely high-energy neutrino coming from the Northern Hemisphere. Neutrinos of this type reach IceCube after passing through Earth, thus filtering out all background. For this reason, the uncertainties are smaller: typical pointing errors are less than 0.5°. They occur four to six times per year. The first alert was sent in July 2016.

[3]This is a process analogous to the Cherenkov radiation, that forms roughly in the same way.

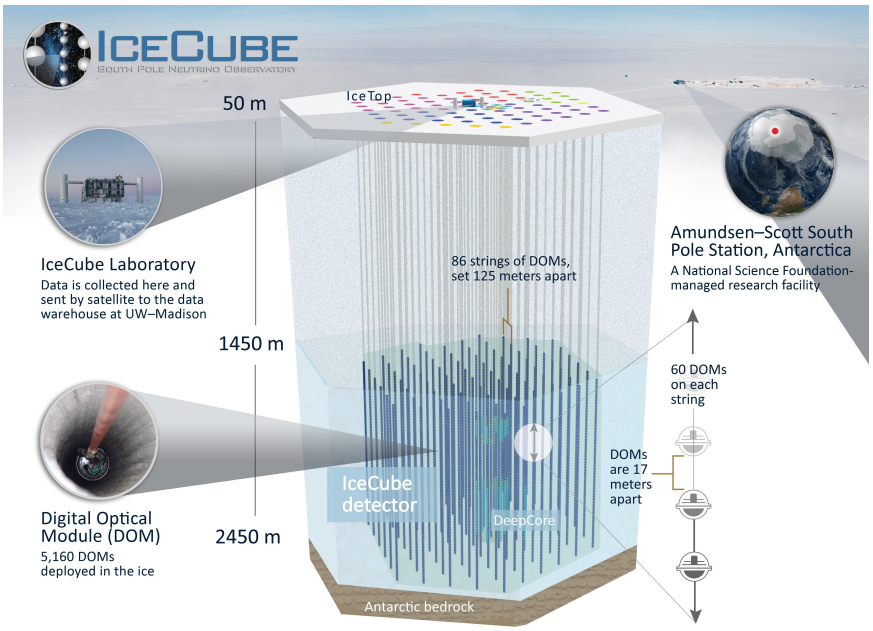

Figure 4.1: DOMs are the digital optical modules, each with a photomultiplier and relative electronics; there are in total 5160 of these. DeepCore is the center array, that has a major density of detectors. IceTop is composed of a total of 81 DOMs organized on the surface, for the detection of the cosmic ray and the calibration of IceCube. Image credit: IceCube.

In November 2013 it was announced that 28 neutrinos were detected, which likely originated outside the Solar System. Among those, a pair of high-energy neutrinos in the PeV range, making them among the highest energy neutrinos currently discovered. The pair were nicknamed "Bert" and "Ernie". Later in 2013, the number of detections increased to 37, including a new high-energy neutrino at 2PeV given the name of "Big Bird".

In July 2018, IceCube scientists announced that they had traced an EHE neutrino that hit their detector in September 2017. They linked this to the blazar TXS 0506+056 located 5.7 billion light-years away. This was the first time that a neutrino detector had been used to locate an object in space.

Finally, in November 2022 IceCube announced the detection of a neutrino emitted by the active galactic nucleus of Messier 77 (also known as NGC 1068). This AGN and the blazar above, are (probably) two of the four known sources for astrophysical neutrinos[4]. In figure 4.2 there is the graphic rendering of the detection of "Ernie".

[4]The other two are the Sun and the supernova SN 1987A.

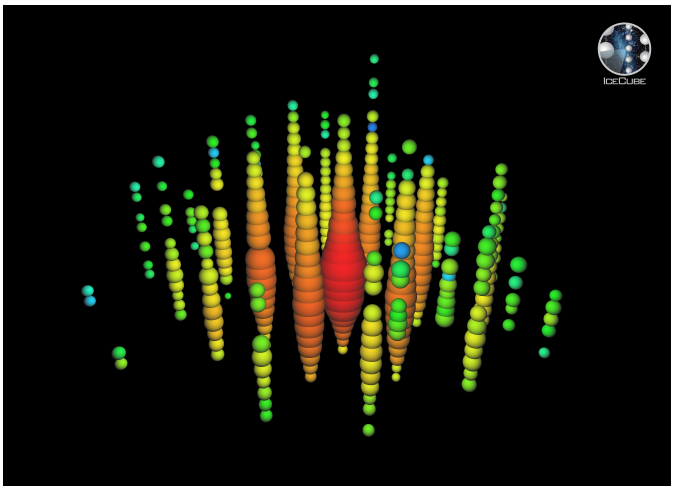

Figure 4.2: Each dot represents an optical module in the IceCube neutrino detector. The colored spots indicate that the optical modules detected a particle. Red is where the particle interaction began and the size of the colored spot refers to the intensity of the emitted Cherenkov light. Image credit: IceCube.

4.2 IceCube events for the evidence of astrophysical neutrinos

4.2.1 The 2013 IceCube Collaboration

In 2013, Aartsen et al.[18] report data obtained between 2010 and 2012 with the IceCube neutrino detector that reveals 28 events at energies between 30 TeV and 1.2 PeV. As said before, it was found that two of those neutrinos have energy of $\sim$ PeV, for which we expect extraterrestrial origins. The expected event from atmospheric muons and neutrinos, calculated in the same amount of time of the data taking, was $10.6^{+5.0}_{-3.6}$, below the event captured by IceCube.

Four events started were down-going, consistent with the properties of the expected 6.0 ± 3.4 background atmospheric muons, as measured from a control sample of penetrating muons in data. Muons form in the atmosphere due to the interaction between this and cosmic rays; the subsequent formed pions decay in the way we have already seen (the decays 3.12 and 3.13): For this reason, they form an atmospheric neutrino background that in the case of this study, have to take in account. The points at which the remaining events were first observed were uniformly distributed throughout the detector. This is consistent with expectations for neutrino events and inconsistent with backgrounds from penetrating muons or with systematic detector errors.

To exclude the background origins of the events, the study has modeled an atmospheric-only neutrino-flux, following [28]. This predicts, on average, a 6.1 background neutrinos from pions, kaons, and charm[5], in addition to the muon background. The final result is that the background origins of the total 28 events deviate from a "standard level" with a $\sim 4\sigma$, depending on the statistical method adopted. Furthermore, the energy spectrum, angular distribution, and shower-to-muon track ratio of the observed

[5]Kaon is a type of meson, and charm is a type of quark.

events strongly constrain the possibility that events are entirely of atmospheric origin. The angular distribution of the events is consistent with isotropic assumption, while atmosphere origins would lead to an anisotropic distribution. Neutrino atmospheric flux scale as $\sim E^{-3.7}$ (see [3]), while the data are well described by an E^{-2} neutrino spectrum with an all-flavour normalization of:

$$E^2\phi(E) = (1.2 \pm 0.4) \times 10^{-8}\ GeV\ cm^{-2}\ s^{-1}\ sr^{-1}$$

A flux at this level would have been expected to generate an additional three to six events in the 2 to 10 PeV range; the lack of such events in the sample may indicate either a softer spectrum or the presence of a break or cutoff above the PeV energies.

Reconstructing a precise direction in the sky, to possibly link a source for these events, was not possible due to the low angular resolution. Despite that, the study confirms the presence of an extraterrestrial neutrino flux at high energies and for this reason, the GCN/TAN network was developed to facilitate the detection of these interesting events.

4.2.2 Neutrino in the direction of TXS 0506+056

The event IceCube-170922A detected on 22 September 2017 was coincident in direction and time with a gamma-ray flare from the blazar TXS 0506+056. The event was targeted as an EHE alert, of an estimated energy of 290TeV.

The blazar is a north hemisphere source located at right ascension (RA) 77.3582° and declination (Dec) +5.69314° (J2000 equinox) and the best fitting for the event is of RA $77.43^{+0.95}_{0.65}$ and Dec $5.72^{+0.50}_{0.30}$ (both in degrees), that correspond to a 90% containment region. The enhanced γ-ray activity of the blazar has been observed since April 2017 by the Large Area Telescope (LAT) on the Fermi Gamma-ray Space Telescope. The significance of the spatial and temporal coincidence of the high-energy neutrino and the blazar flare is estimated to be at the 3σ level (see [17]).

To prove the possibility that TXS 0506+056 could be a neutrino source, in [17] used two model-independent methods to the data from the sky region of the blazar, collected between 2008 and 2017. A high-significance point source detection can require as few as two or three, or as many as 30, signal events to stand out from the background, depending on the energy spectrum and the clustering of events in time. The result is that there is a correlation between the source and some events during the 9-year time box of data taking. Both methods give a neutrino spectrum well described by a E^{-2} trend and the flux normalization at 100TeV:

$$\phi_{100} = 0.8^{+0.5}_{-0.4} \times 10^{-16}\ TeV^{-1}\ cm^{-2}\ s^{-1}$$

There was only a mismatching excess of neutrinos from 2012 to 2015. The study found an excess of high-energy neutrino events with respect to atmospheric backgrounds, between September 2014 and March 2015. This constitutes 3.5σ evidence for neutrino emission from the direction of TXS 0506+056, independent of and prior to the 2017 flaring episode. This suggests that blazars are identifiable sources of the high-energy astrophysical neutrino flux, and confirms that the event IceCube-170922A wasn't a coincidence.

It also calculated the all-flavor neutrino flux and combined that with the redshift of the source, calculating the isotropic neutrino luminosity (averaged over 158 days):

$$L_\nu = 1.2^{+0.6}_{-0.4} \times 10^{47}\ erg\ s^{-1}$$

The isotropic γ-ray luminosity, taken from all Fermi-LAT observations during the same period [16], between 0.1TeV and 100 TeV is lower:

$$L_\gamma = 0.28 \times 10^{47}\ erg\ s^{-1}$$

Since γ-rays are expected to be produced in the same processes that produce neutrinos, a higher luminosity in neutrinos than in gamma rays could imply that a substantial fraction of the gamma rays related to the neutrino production are either absorbed or arriving at energies above or below the Fermi-LAT energy band.

4.2.3 Neutrino from NGC 1068

The galaxy NGC 1068, also known as M77, is a Seyfert 2 galaxy. Recently, in [19] there seems to be evidence for neutrino emission from this source. It is found that there is an excess of 79^{+22}_{-20} neutrinos at TeV energies, with a global significance of 4.2γ. The excess was found by studying the data from 2011 to 2020.

Assuming that NGC 1068 is a neutrino source is a strong assumption, but if it were true it would be interesting. This is because the source is classified as radio-loud, and this could mean that also in this AGN is possible the presence of a hadronic component accelerated to relativistic energies.

The muon neutrino flux calculated at 1TeV is of:

$$\phi_{\nu_\mu}^{1TeV} = (5.0 \pm 1.5) \times 10^{-11}\ TeV^{-1}\ cm^{-2}\ s^{-1}$$

that is 3 times higher if we consider the all-flavour flux. Assuming a distance of NGC 1068 of $14.4 Mpc$, the averaged isotropic neutrino luminosity is:

$$L_\nu = (2.9 \pm 1.1) \times 10^{42}\ erg\ s^{-1}$$

that is an order of magnitude higher than the equivalent γ-ray luminosity of:

$$L_\gamma = 1.6 \times 10^{41}\ erg\ s^{-1}$$

taken from all Fermi-LAT observations during the same period, between 100GeV and 100 MeV([7]-[4]). The neutrino luminosity also exceeds the upper limits reported above 200GeV (see [5]). This can be explained remember the AGN classification: Seyfert 2 AGN are the ones in which the central region is obscured by the torus. So, the discrepancy of luminosity could tell us that the neutrinos are produced in a region with high absorption for the γ-ray. If this is true, NGC 1068 could be a neutrino source.

Chapter 5

Conclusion

Detection of more astrophysics neutrinos could open a new way to examine our universe, especially the most extreme and prohibitive environments that can't be studied only with photons. Although there is only three kinds of sources that are confirmed neutrino emitters in the cosmos (the blazar TXS 0506+056, the nearest star, the Sun, and the supernova SN 1987A), we have to take into consideration that neutrinos are very difficult to detect, and we "just began" the observation in this way. AGNs are among the most promising candidates for contributing to an astrophysical neutrino flux, so the next years could be very interesting in the field of multimessenger astrophysics.

Appendix A

Neutrinos

In the first quarter of the last century, in the study of beta decay, there was a problem: it seems to be a violation of the energy conservation law. It was thought that the outgoing electrons have a fixed energy, but different experiments made in particular by Lise Meitner, Otto Hahn, and James Chadwick in 1914, have demonstrated that electrons have a continuum spectra energy. In successive years were proposed theories to face this contradiction, and the correct one was a postulation by Wolfgang Pauli, in his famous letter "Dear radioactive ladies and gentlemen" sent in 1930. To "save" the law of energy conservation, he proposed the existence of a light, neutral, weakly interacting particle that accompanies the electron in the decay.

Three years later, Enrico Fermi developed the beta decay theory and gave the name "neutrino" to this ambiguous and not yet discovered particle. The first detection of the neutrino (more precisely, it was detected electron anti-neutrino) was in 1956 by the Reines and Cowan experiment, which consisted of putting a detector near the nuclear plant of Hanford.

Neutrino is a fundamental particle almost massless (< 1eV for the sum of all flavors), so it can reach easily high velocity, very near to the speed of light. It has a spin of 1/2 and has no electric charge. As they interact only with weak interaction, which is important only in short distances, they can pass through matter without interacting at all; every second we are traversed roughly by thousand trillions of neutrinos every second.

The neutrino has 3 different "flavors", depending on which are its "parent" lepton: electron, pion, or tau. The discovery of the pion-neutrino was thanks to M. Schwartz, L. Lederman, and J. Steinberger in 1962 from BNL (Brookhaven National Laboratory), while tau-neutrino was first detected in 2000 at Fermilab by DONUT experiment. The flavors of neutrinos can "oscillate", that is one neutrino can change flavor over time. This is an important and surprising process, that requires a massive neutrino; as seen in section 4.1 on page 22, this discovery brought a Nobel prize in 2015. Despite that, the mass of the single neutrino is still unknown, due to the difficulty of building an experiment to determine that. How neutrinos take their mass is also more mysterious because they don't do that through interactions with the Higgs boson. In the Standard Model, this is the particle that gives mass to others. One theory predicts that the neutrino has a very heavy partner called "sterile neutrino" that exists for a very brief time, and that interacts with the Higgs boson. Then with a "seesaw" mechanism, the lighter neutrino is formed from his heavy partner's mass. The mechanism consists of the fact that as the mass of the massive partner goes up, the mass of the light neutrino

goes down; this seesaw relationship has not yet been experimentally verified.

Sterile neutrinos are so-called for their theorized nature: they can interact only with the gravitational field, making them practically invisible. For this reason, scientists are not sure that there are only three neutrino flavors, but today there isn't evidence for addictive flavors.

Other unresolved mysteries of the neutrinos are the fact that we are not sure if they are Dirac or Majorana particles, which would be the lightest neutrinos, and the fact that neutrinos are only left-handed.

Bibliography

[1] Lawrence A. and Elvis M. "Obscuration and the various kinds of Seyfert galaxies". In: *Astrophysical Journal* 256 (1982).

[2] Wilson A.S. and Colbert E.J.M. "The Difference between Radio-loud and Radio-quiet Active Galaxies". In: *The Astrophysical Journal* 438 (1995).

[3] Mark G Aartsen et al. "Observation and Characterization of a Cosmic Muon Neutrino Flux from the Northern Hemisphere using six years of IceCube data". In: *The Astrophysical Journal* 833.1 (2016).

[4] Soheila Abdollahi et al. "Fermi large area telescope fourth source catalog". In: *The Astrophysical Journal Supplement Series* 247.1 (2020).

[5] Victor A Acciari et al. "Constraints on gamma-ray and neutrino emission from NGC 1068 with the MAGIC telescopes". In: *The Astrophysical Journal* 883.2 (2019).

[6] F.A. Aharonian. "TeV gamma rays from BL Lac objects due to synchrotron radiation of extremely high energy protons". In: *New Astronomy* 5.7 (2000), pp. 377–395.

[7] Marco Ajello et al. "The fourth catalog of active galactic nuclei detected by the Fermi Large Area Telescope". In: *The Astrophysical Journal* 892.2 (2020).

[8] M. Nakamura Asada. "The Structure of the M87 Jet: A Transition from Parabolic to Conical Streamlines". In: *The Astrophysical Journal* 745.28 (2012).

[9] Rudak B. Begelman M.C. and Sikora M. "Consequences of relativistic proton injection in active galactic nuclei". In: *Astrophysical Journal* 362 (1990).

[10] D.G. Payne Blandford. "Hydromagnetic flows from accretion discs and the production of radio jets". In: *Monthly Notices of the Royal Astronomical Society* 199 (1982), pp. 883–903.

[11] R.L. Znajek Blandford. "Electromagnetic extraction of energy from Kerr black holes". In: *Monthly Notices of the Royal Astronomical Society* 179 (1977), pp. 433–456.

[12] Netzer H. Blandford R.D., Courvoisier T.J.L. Woltjer L., and M. Mayor, eds. *Active Galactic Nuclei*. 1990.

[13] Rees. M.J. Blandford R.D. "Extended and compact extragalactic radio sources: interpretation and theory". In: *Physica Scripta* 17 (1978).

[14] R.J. Gould Blumenthal. "Bremsstrahlung, Synchrotron Radiation, and Compton Scattering of High-Energy Electrons Traversing Dilute Gas". In: *Reviews of Modern Physics* 42 (1970), pp. 237–271.

[15] Harris D.E. Böttcher M. and Krawczynski H. *Relativistic jets from active galactic nuclei*. 2012.

[16] IceCube Collaboration et al. "Multimessenger observations of a flaring blazar coincident with high-energy neutrino IceCube-170922A". In: *Science* 361.6398 (2018).

[17] IceCube Collaboration et al. "Neutrino emission from the direction of the blazar TXS 0506+056 prior to the IceCube-170922A alert". In: *Science* 361.6398 (2018).

[18] IceCube Collaboration*. "Evidence for High-Energy Extraterrestrial Neutrinos at the IceCube Detector". In: *Science* 342.6161 (2013).

[19] IceCube Collaboration*† et al. "Evidence for neutrino emission from the nearby active galaxy NGC 1068". In: *Science* 378.6619 (2022).

[20] Zirbel E.L. and Baum S.A. "On the FR I/FR II dichotomy in powerful radio sources: analysis of their emission-line and radio luminosities". In: *The Astrophysical Journal* 448 (1995).

[21] Aharonian F.A. *Very high energy cosmic gamma radiation: a crucial window on the extreme Universe*. 2004.

[22] Miller L. Fabbiano G., Longair M. Trinchieri G., and Elvis M. "Erratum-an X-Ray Survey of a Complete Sample of 3CR Radio Galaxies". In: *Astrophysical Journal* 283 (1984).

[23] Willner S.P. Fabbiano G. and Elvis M. Carleton N.P. "The highly obscured nucleus of 3C 219". In: *Astrophysical Journal* 304 (1986).

[24] Riley Fanaroff. "The morphology of extragalactic radio sources of high and low luminosity". In: *Monthly Notices of the Royal Astronomical Society* 167 (1974), 31P–36P.

[25] Hill G.J. and Lilly S.J. "A change in the cluster environments of radio galaxies with cosmic epoch". In: *The Astrophysical Journal* 367 (1991).

[26] A. Treves Ghisellini L. Maraschi. "Inhomogeneous synchrotron-self-Compton models and the problem of relativistic beaming of BL Lac objects". In: *Astronomy and Astrophysics* 146 (1985), pp. 204–212.

[27] Padovani P. Ghisellini G. and Maraschi L. Celotti A. "Relativistic bulk motion in active galactic nuclei". In: *Astrophysical Journal* 407 (1993).

[28] T. Honda M. Kajita, Midorikawa S. Kasahara K., and Sanuki T. "Calculation of atmospheric neutrino flux using the interaction model calibrated with atmospheric muon data". In: *Physical Review D* 75.4 (2007).

[29] Sramek R. Kellermann K.I., Shaffer D.B. Schmidt M., and Green R. "VLA Observations of Objects in the Palomar Bright Quasar Survey". In: *Astronomic Journal* 98 (1989).

[30] Rees M.J. "Appearance of relativistically expanding radio sources". In: *Nature* 211 (1966).

[31] Dimitrakoudis S. Petropoulou M., Mastichiadis A. Padovani P., and Resconi E. "Photohadronic origin of Formula-ray BL Lac emission: implications for IceCube neutrinos". In: *Monthly Notices of the Royal Astronomical Society* 448 (2015).

[32] Krolik J.H. Pier E.A. "Infrared Spectra of Obscuring Dust Tori around Active Galactic Nuclei. II. Comparison with observations". In: *The Astrophysical Journal* 418 (1993).

[33] Krolik J.H. Pier E.A. "Radiation-Pressure–supported Obscuring Tori around Active Galactic Nuclei". In: *The Astrophysical Journal* 399 (1992).

[34] G. Cotter Potter. "Synchrotron and inverse-Compton emission from blazar jets - II. An accelerating jet model with a geometry set by observations of M87." In: *Monthly Notices of the Royal Astronomical Society* 429 (2013), pp. 1089–1205.

[35] F. Ryde Poutanen J.H. Krolik. "The nature of spectral transitions in accreting black holes - The case of CYG X-1." In: *Monthly Notices of the Royal Astronomical Society* 292 (1997), pp. 21–25.

[36] Prestage R.M. and Peacock J.A. "The cluster environments of powerful radio galaxies". In: *Monthly Notices of the Royal Astronomical Society* 230 (1988).

[37] Antonucci R.R.J. and Miller J.S. "Diffuse pulmonary hemorrhage: a review and classification". In: *The Astrophysical Journal* 297 (1985).

[38] Eales S.A. Rawlings S. Saunders R. and Mackay C.D. "The relations between radio and forbidden [O III]-emission line luminosities in FRII radiogalaxies". In: *Monthly Notices of the Royal Astronomical Society* 240 (1989).

[39] G.S. Vila Romero F.L. Vieyro. "Non-thermal processes around accreting galactic black holes". In: *Astronomy and Astrophysics* 519.109 (2010).

[40] S. Markoff Romero M. Boettcher and F. Tavecchio. "Relativistic Jets in Active Galactic Nuclei and Microquasars". In: *Space Science Reviews* 207.1-4 (2017), pp. 5–61.

[41] Lightman A.P. Rybicki G.B. *Radiative processes in astrophysics.* 1979.

[42] Baum S.A. and Heckman T. "Extended optical line emitting gas in powerful radio galaxies-Statistical properties and physical conditions". In: *The Astrophysical Journal* 336 (1989).

[43] Phinney E.S. Sanders D.B., Neugebauer G. Soifer B.T., and Matthews K. "Continuum Energy Distributions of Quasars: Shapes and Origins". In: *The Astrophysical Journal* 347 (1989), p. 29.

[44] Heckman T.M. Smith E.P., Romanishin W. Bothun G.D., and Balick B. "On the Nature of QSO Host Galaxies". In: *The Astrophysical Journal* 306 (1986).

[45] Padovani Urry. "Unified Schemes for Radio-Loud Active Galactic Nuclei". In: *Publications of the Astronomical Society of the Pacific* 107.715 (1995), pp. 803–815.

[46] Cohen M.H. Vermeulen R.C. "Superluminal motion statistics and cosmology". In: *The Astrophysical Journal* 430 (1994).

Acknowledgments

I would thank Professor Mauro D'Onofrio, the supervisor, and Doctor Paola Marziani, the co-supervisor, for their help, patience, time, and disposability.

A huge thanks to my family, for their patience towards me in the past years, for all the help and love given to me, and for pushing me to continue studying.

A pruppu thanks to my girlfriend, partner in crime, and best friend Benny, who helped me to bring out the best part of me, and is supporting me and making me have fun for four years. Without her, I wouldn't be here writing these words.

Thanks to Bubu, the best fisherman and failed engineer I ever known, Trent, the number 1 Berusconi fan and future champion of (low quality) puns, Leu, my nicest namesake who stole my name and the best nerd I have known, Kristian, my pizza-making mate who renamed me Aurelio, Raffa, mate in speculative discussions about our universe, Juju, my fake sister, Alicio, my Jappo Besto Friendo, Carol, the only girls who drinks more than me, and Norris, the sweetest dog that I could have. Probably, without them, I would be a totally different person and my life would have been boring.

Finally, I want to thank the best part of me, that has emerged in recent years, who taught me that I'm not as stupid as I think, who made me understand how much I'm worth, and who I hope will bring me great satisfaction, sooner or later.